Enabling 100C Fast-Charging Bulk Bi Anodes for Na-Ion Batteries

Young-Hoon Kim[1,†], Jae-Hyun An[1,†], Sung-Yeob Kim[1], Xiangmei Li[1], Eun-Ji Song[2], Jae-Ho Park[3], Kyung Yoon Chung[3,4], Yong-Seok Choi[5,6], David O. Scanlon[5,6], Hyo-Jun Ahn[2,*], Jae-Chul Lee[1,7*]

[1]Department of Materials Science and Engineering, Korea University, Seoul 02841, South Korea

[2]Department of Materials Engineering and Convergence Technology, Gyeongsang National University, Jinju 52828, South Korea

[3]Energy Storage Research Center, Korea Institute of Science and Technology, Seoul 02792, South Korea

[4]Division of Energy & Environment Technology, KIST School, Korea University of Science and Technology, Seoul 02792, South Korea

[5]Department of Chemistry, University College London, 20 Gordon Street, London, WC1H 0AJ, UK

[6]Thomas Young Centre, University College London, Gower Street, London WC1E 6BT, UK

[7]Institute of Green Manufacturing Technology, Korea University, Seoul 02841, South Korea

†These authors contributed equally to this work.

*To whom correspondence should be addressed: Hyojun Ahn (email: ahj@gnu.ac.kr),

This article has been accepted for publication and undergone full peer review but has not been through the copyediting, typesetting, pagination and proofreading process, which may lead to differences between this version and the Version of Record. Please cite this article as doi: 10.1002/adma.202201446.

Jae-Chul Lee (email: jclee001@korea.ac.kr)

Abstract: It is challenging to develop alloying anodes with ultrafast charging and large energy storage using bulk anode materials, because of the difficulty of carrier-ion diffusion and fragmentation of the active electrode material. Herein, we report a rational strategy to design bulk Bi anodes for Na-ion batteries that feature ultrafast charging, long cyclability, and large energy storage without using expensive nanomaterials and surface modifications. We found that bulk Bi particles gradually transform into a porous nanostructure during cycling in a glyme-based electrolyte, whereas the resultant structure stores Na ions by forming phases with high Na diffusivity. These features allowed the anodes to exhibit unprecedented electrochemical properties; the developed Na–Bi half-cell 379 $mAhg^{-1}$ (97% of that measured at 1C) at 7.7 Ag^{-1} (20C) during 3500 cycles. It also retained 94% and 93% of the capacity measured at 1C even at extremely fast-charging rates of 80C and 100C, respectively. The structural origins of the measured properties were verified by experiments and first-principles calculations. The findings of this study not only broaden our understanding of the underlying mechanisms of fast-charging anodes, but also provide basic guidelines for searching battery anodes that simultaneously exhibit high capacities, fast kinetics, and long cycling stabilities.

1. Introduction

Alloying anodes have large theoretical capacities, but they are being criticized for their limited practical capacity, poor rate performance, and poor cycling stability. To overcome these shortcomings, most studies have implemented strategies based on nanoscale materials in the form of nanoparticles or nanowires[1]. However, even with the use of nanoscale materials, the large volume changes associated with charging and discharging cause the fragmentation of the anode material[2] , decreasing their capacities and cycling lifetimes. The coating and doping of anode nanomaterials are among the various methods proposed to address this problem[3]. However, these methods are complex and expensive, and the overlayer coated on the anode nanomaterials may hinder the fast transport of carrier ions. Another approach based on the reaction between an anode material and electrolyte has also been reported[4]. This method induces the spontaneous restructuring of a bulk anode material into a three-dimensional (3D) porous nanostructure during battery cycling with a glyme-based electrolyte[4b-e]. Although the short diffusion distance in thus-formed nanostructure is beneficial for improving the rate performance of the anode, its energy capacity still rapidly decreases with increasing current density (C-rate)[3a, 3b, 5]. This indicates that a strategy based on reducing the diffusion distance alone is not sufficient to simultaneously improve the energy capacity, rate capability, and cycling stability of alloying anodes.

To determine another variable governing the kinetics of carrier-ion diffusion at high C-rates, it is necessary to investigate why the practical capacity of the anode decreases with increasing C-rate. At low C-rates, carrier ions diffusing into the anode can fully contribute to electrode reactions by combining with electrons flowing from an external circuit, thereby

fully charging the anode. However, as the current density increases during the fast charging of the anode, the flux of carrier ions flowing into the anode does not increase at the same rate as the applied current density. Accordingly, beyond the maximum C-rate that allows easy charging, the anode is depleted of carrier ions and thus becomes negatively charged, which hinders any additional current inflow into the anode, thus limiting charge storage. This critical charging rate is often called the "diffusion-limited C-rate" (DLC)[6]. The above analysis suggests that in addition to the structural configuration that ensures a short diffusion distance, a material that produces phases with high diffusivity is also essential for suppressing the onset of the DLC and realizing fast-charging anodes.

Electric charge is stored in the anode via the phase transition, during which various intermediate phases with different diffusivities are formed. Because the diffusivity (D) of carrier ions in an intermediate phase is inversely related to its electrical resistivity (ρ) (i.e., $D \propto 1/\rho$)[7], anode materials that form phases with high electrical conductivity are beneficial for mitigating the onset of the DLC, thereby facilitating fast charging. Among the various battery systems, the Na–Bi system features a simple phase transition during charging/sodiation, i.e., Bi $\rightarrow$ NaBi $\rightarrow$ Na_3Bi[8]. In contrast to most lithiated and sodiated phases formed during the electrode reactions corresponding to charging, both NaBi and Na_3Bi exhibit high electrical conductivities, as will be shown later. Furthermore, bulk Bi can spontaneously form a 3D porous nanostructure during battery cycling in the presence of an appropriate electrolyte[4b, 4e]. Therefore, this nanostructured material can benefit from both the short diffusion distance (x) and high diffusivity (D) of the NaBi and Na_3Bi phases, which reduce the charging time (t) according to the relation $t \propto x^2/D$ and retard the onset of the

DLC. Thus, the Na–Bi system could be an ideal testbed material to investigate the potential of the above scenario in simultaneously improving the rate performance, energy capacity, and cycling stability of an anode.

In this study, an extremely fast-charging Bi anode with large capacity and long cycling lifetime was developed without using expensive nanomaterials and complex surface modifications for application in Na-ion batteries. The developed Na–Bi half-cell delivered 382 and 379 $mAhg^{-1}$ at 10C (3.85 Ag^{-1}) and 20C (7.7 Ag^{-1}), respectively, and ran for more than 6000 and 3500 cycles, respectively. It also steadily exhibited 94% (369 $mAhg^{-1}$) and 93% (364 $mAhg^{-1}$) reversible capacities even at ultrahigh current densities of 30.8 Ag^{-1} (80C) and 38.5 Ag^{-1} (100C), respectively. Experiments and density functional theory (DFT) calculations were performed to verify the structural origin of the measured properties.

2. Results

2.1. Electrochemical properties

Commercial bulk Bi particles were used as received and without any pre-treatments. Bulk Bi particles are polycrystals with sizes of 1–10 μm and a rhombohedral structure (Figure S1, Supporting Information). The anodes used in the Na–Bi half-cell were prepared by mixing bulk Bi particles, multiwalled carbon nanotubes (MWCNTs), and polyvinylidene fluoride (PVdF) in a weight ratio of 70:15:15 (see Methods, Supporting Information). During battery cycling, the repetitive insertion and extraction of Na ions cause Bi particles to fragment into nanoparticles (NPs). Because NPs can coalesce in the presence of an

appropriate electrolyte[9], two types of Na–Bi half-cells were prepared using electrolytes containing two different solvents: 1) ethylene carbonate (EC) mixed with diethyl carbonate (DEC) (hereinafter referred to as the EC/DEC solvent) and 2) dimethoxyethane (DME).

Before we evaluated the rate capabilities of the two different Na–Bi half-cells, the specific capacity of the Bi anode was measured at 1C (=385 mAg^{-1}). The Bi anode exhibited a capacity of 393 $mAhg^{-1}$ at 1C, which slightly exceeds the theoretical capacity of Bi (385 $mAhg^{-1}$, corresponding to the formation of Na_3Bi), and it was attributed to the energy storage capability of the MWCNTs (40 $mAhg^{-1}$ at 1C, see Figure S2, Supporting Information). This measured capacity (393 $mAhg^{-1}$) at 1C is used as the reference value for discussing the electrochemical properties of the Bi anode and is hereinafter referred to as the "initial capacity". When measuring the specific capacity as a function of the C-rate for the Na–Bi half-cell with the EC/DEC solvent, the specific capacity instantly decreased with battery cycling and converged to almost zero after 20 cycles at 1C (Figure S3, Supporting Information). Conversely, the Na–Bi half-cell with DME stored 382 $mAhg^{-1}$ (97% of its initial capacity) at 8C (**Figure 1**a). It also retained 94% (369 $mAhg^{-1}$) and 93% (364 $mAhg^{-1}$) of its initial capacity even at 80C and 100C, respectively, which then decreased to 83% energy retention (325 $mAhg^{-1}$) at 150C (corresponding to 24 s to full charge) (for the relevant voltage–capacity profiles, see Figure S4, Supporting Information). The rate performance and energy capacity of the bulk Bi anode developed in this study were better than those of previously reported Bi anodes (Figure 1b) prepared using various Bi NPs with coating and doping modifications[4b, 5b, 10]. The extraordinary rate capability and energy capacity of the

developed anode indicate that the reversible formation of Na_3Bi was feasible at the Bi anode at extremely high current densities.

Next, we evaluated the cycling stability of the Na–Bi half-cells by measuring the changes in the specific capacity of the Bi anode in two electrolytes containing different solvents (Figure 1c). For the Na–Bi half-cell with the EC/DEC solvent, the capacity abruptly declined to almost zero after the 20th cycle, even at a low C-rate (1C) (for the voltage–capacity profiles, see Figure 1d). This capacity reduction, which is common for alloying anodes, was attributed to the fragmentation of Bi particles associated with repeated cycling, and it has been discussed extensively in earlier studies[2]. In contrast, the Na–Bi half-cell with the DME solvent stored 382 $mAhg^{-1}$ at 10C (3.85 Ag^{-1}), which slightly decreased to 378 $mAhg^{-1}$ after 6000 cycles (Figure S5, Supporting Information). At a higher current rate of 20C, the half-cell still delivered 379 $mAhg^{-1}$, which then gradually decreased to 360 $mAhg^{-1}$ after 3500 cycles with an average capacity loss of 0.0014% per cycle (for the voltage–capacity profiles, see Figure 1e). Similar cycling stabilities and energy capacities were observed even at extremely high C-rates. For example, the Bi anode retained 96% (378 $mAhg^{-1}$) of its initial capacity over 700 cycles at 32C (Figure S6, Supporting Information). These results demonstrated the suitability of micrometer-sized bulk Bi particles as active anode materials for Na-ion batteries with the simultaneously improved rate performance, capacity, and cycling stability values. Therefore, it is essential from the perspective of research as well as practicality to elucidate the structural and electrical origins of the excellent electrochemical properties of Bi anodes.

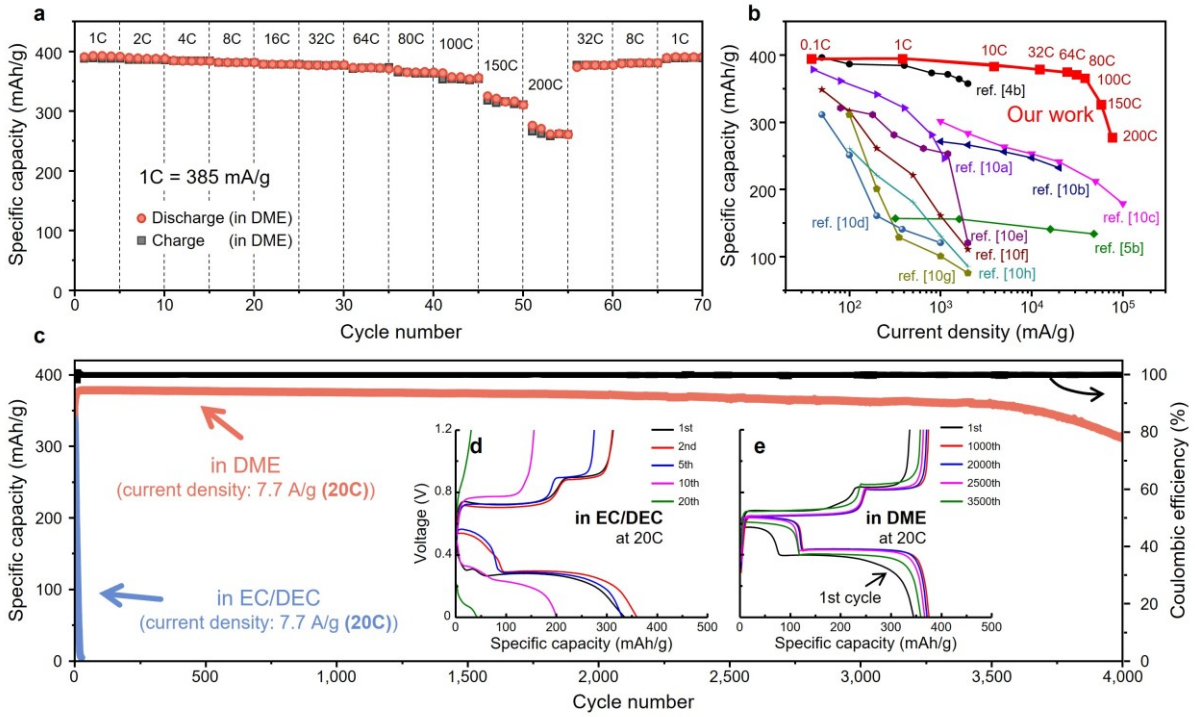

Figure 1. Electrochemical performances of Na–Bi half-cells. (a) Changes in specific capacity of Na–Bi half-cells measured at various C-rates using an electrolyte containing DME. Note that the capacity values in (a) were measured after running the first 50 cycles at 1C to induce a complete transformation of bulk Bi particles to a porous nanostructure; (b) comparison of the rate capability of the developed Bi anode with those obtained from other Bi-based anodes reported in previous studies; (c) changes in the specific capacity of Na–Bi half-cell with DME solvent measured at 20C as a function of the battery cycle, with capacity changes in Na–Bi half-cell with the EC/DEC solvent measured at 20C shown for comparison; and changes in the measured voltage–capacity profiles of Na–Bi half-cells in electrolytes containing (d) EC/DEC (at 20C) and (e) DME (at 20C), where all measurements were performed after running first cycle at 0.1C for stabilization.

The repetitive insertion and extraction of Na ions associated with charging and discharging cause large volume changes in the Bi anode. This unavoidable volumetric change can cause the fragmentation of bulk Bi particles into NPs, which can considerably alter the initial structure/morphology of the Bi anode, depending on the electrolyte solvent used. For the Bi anode cycled in the electrolyte with the EC/DEC solvent, the fragmented Bi NPs remained physically and electrically isolated (Figure S7, Supporting Information), which rapidly decreased the energy capacity and cycling lifetime of the anode, as shown in Figure 1c. Conversely, the high cycling stability and energy capacity of the Na–Bi cells with the DME solvent were in sharp contrast to the rapidly decaying trend observed for the cells with the EC/DEC solvent under the same conditions (Figure 1c).

The improved properties of the Na–Bi cells with the DME solvent must be related to the structure of the Bi anode. **Figure 2** shows a series of images recorded using the Bi anodes extracted from the Na–Bi half-cells subjected to cycling in the DME-containing electrolyte. Notably, repetitive charging and discharging prompted the gradual evolution of the bulk Bi particles/flakes into a 3D porous nanostructure; the extraction of Na ions after the first desodiation changed the initial smooth Bi flakes (Figure 2a and 2e) into a nanostructure with loosely connected Bi NPs (Figure 2b and 2f). With further cycling, the structure gradually evolved into a 3D porous nanostructure characterized by large free spaces and thin struts with thicknesses of 100–300 nm (Figure 2c, 2d, 2g, and 2h). These results indicate that the seemingly detrimental and undesirable fragmentation behavior of the anode material could be

utilized to obtain the required NPs for constructing a 3D porous nanostructure via the coalescence process during subsequent battery cycling.

The porous Bi nanostructure in Figure 2 can affect the electrochemical properties of the anode in various ways. First, the free spaces in the porous nanostructure could alleviate the accumulation of residual stresses at the anode during charging/sodiation, which prevents the self-limiting tendency of Na diffusion[11], and thus improves the energy capacity. Second, a-few-hundred-nanometer thick struts of the porous nanostructure shorten the diffusion distance, which can improve the rate performance. Third, the large surface of the porous nanostructure facilitates the surface diffusion of carrier ions (typically 2–3 orders of magnitude faster than lattice diffusion[12]), further improving the rate performance. Finally, the porous nanostructure is obtained by the spontaneous coalescence of Bi NPs and thus is chemically stable, which improves the cycling stability. Overall, the porous nanostructure, on the one hand, provides a pathway for the fast transport of Na ions[13] and on the other hand improves the structural and chemical stability of the anode, enabling large energy storage, fast kinetics, and long cycling stability for the Bi anodes. The next logical question is whether the excellent rate performance displayed by the Bi anode was solely attributable to the geometry of the porous nanostructure. This important issue is discussed in more detail below.

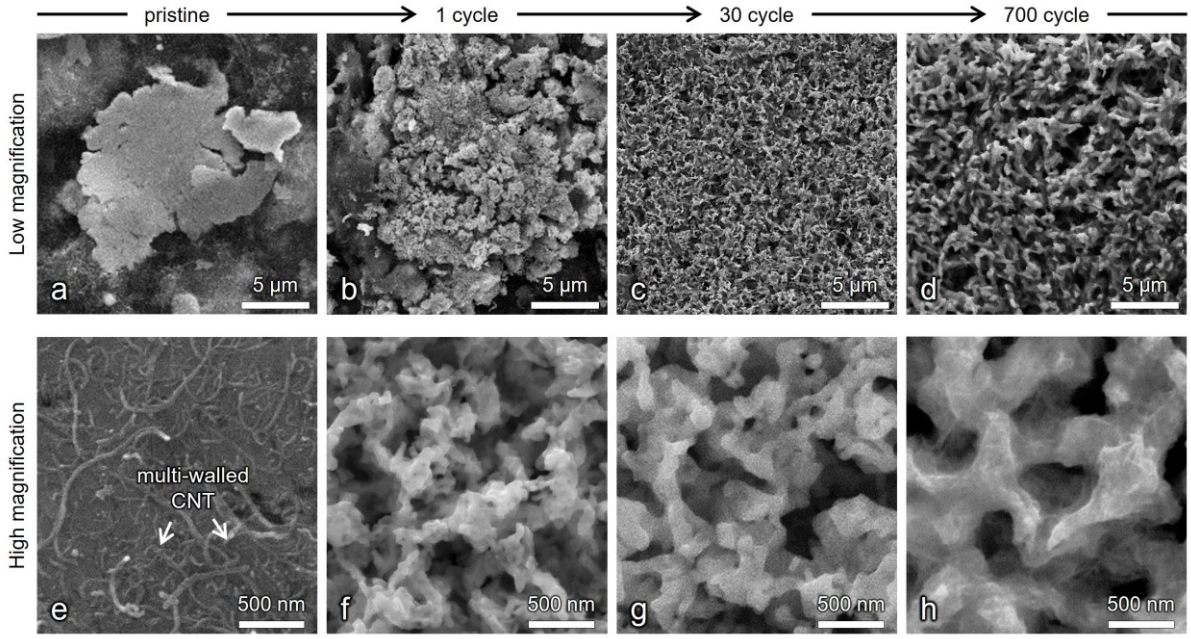

Figure 2. Structural evolution of bulk Bi flakes. Secondary electron images recorded at low (first raw) and high (second raw) magnifications from the surfaces of bulk Bi flakes extracted from pristine anode and anodes subjected to battery cycling in electrolyte containing DME, demonstrating the progressive evolution of bulk Bi flakes into 3D porous nanostructure.

Park et al.[11a, 14] and Choi et al.[15] argued that anode materials that undergo diffusion governed by a diffusion-controlled reaction (DCR) readily form 3D porous nanostructures in the presence of an electrolyte containing DME. Representative systems that follow the DCR mechanism include the Na–Sn, Na–Pb, and Na–Bi systems[13] for alloying anodes, and probably the Na–CuS system[4d] for conversion anodes. Experiments showed that, in addition

to bulk Bi, bulk Sn, Pb, and CuS also evolve to form a 3D porous nanostructure after cycling in the presence of the DME electrolyte solvent (**Figure 3**a–d). Thus, the rate capabilities of the Na–Sn, Na–Pb, Na–CuS, and Na–Bi systems with similar 3D porous nanostructures were compared by measuring the changes in the capacity retention as a function of the C-rate (Figure 3e). Notably, the Na–Bi half-cell stored an electric charge that is close to the initial capacity (393 $mAhg^{-1}$ at 1C) at C-rates of up to 80C, which then decreased to <82% (325 $mAhg^{-1}$) of the initial capacity as the C-rate became greater than 150C. Conversely, for the Na–Sn and Na–Pb half-cells, the capacity decreased to <80% when the C-rates exceeded 10C. Similarly, the capacity of the Na–CuS half-cell began to decrease to <80% at 35C under the same conditions (for the voltage–capacity profiles measured for the Na–Sn, Na–Pb, Na–CuS, and Na–Bi cells at various current densities, see Figure S8, Supporting Information). This suggests that the short diffusion distance of the porous nanostructure was not the only factor that influenced the excellent rate capability of the Bi anode. Considering the relationship ($t \propto x^2/D$) supporting the kinetics of diffusion, we consider the Na diffusivity (D) at the anode during charging to be another important factor affecting the rate performance of the Bi anode.

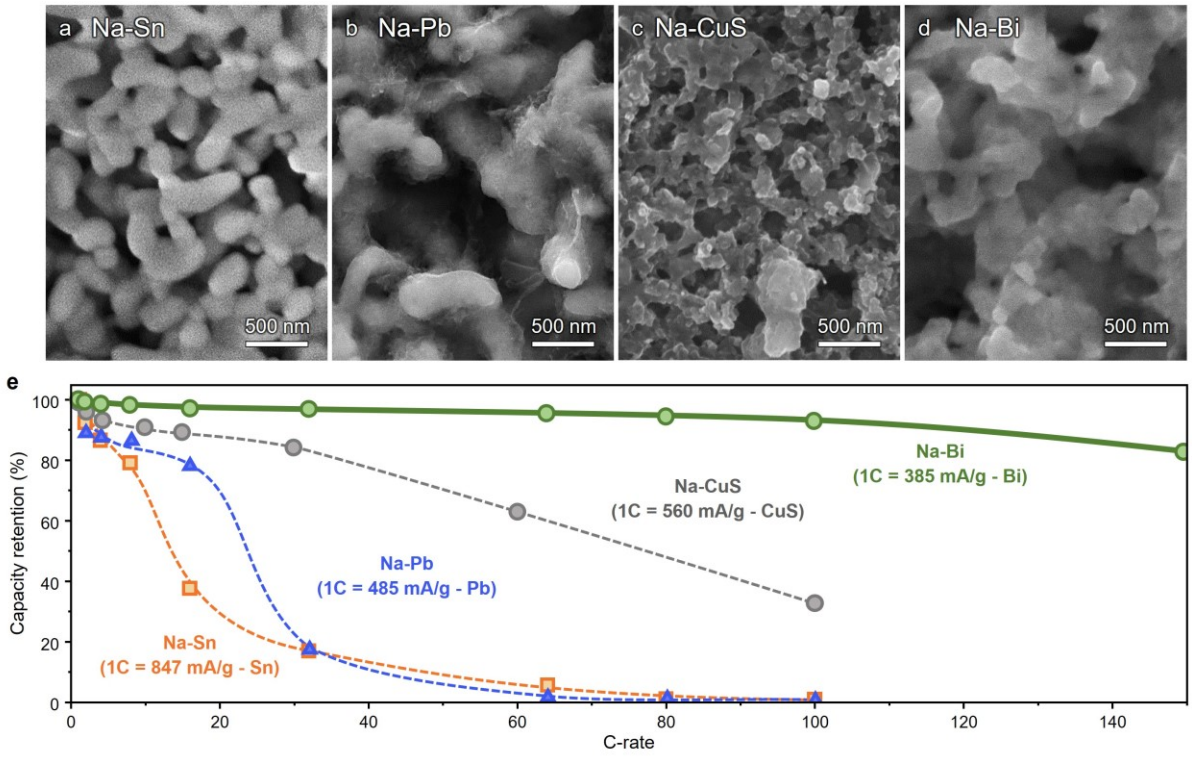

Figure 3. Comparison of capacity retention values of porous nanostructured anodes: 3D porous nanostructures of (a) Sn, (b) Pb, (c) CuS, and (d) Bi anodes extracted from the Na–Sn, Na–Pb, Na–CuS, and Na–Bi half-cells subjected to cycling in DME-containing electrolyte; and (e) changes in the energy retention measured for the Na–Sn, Na–Pb, Na–CuS, and Na–Bi half-cells as a function of the C-rate. Note that the energy retention was defined by the ratio of the capacity measured at a given C-rate to the initial capacity of the anode measured at 1C.

3. Discussion

To elucidate the structural origins responsible for the excellent electrochemical properties of the Bi anode, we addressed three fundamental issues: (1) How do fragmented Bi

NPs spontaneously coalesce to construct the 3D porous nanostructure in the DME electrolyte? (2) Why is the formation of electrically conductive phases important for realizing ultrafast-charging anodes? (3) What is the major energy storage kinetics responsible for the ultrafast transport of Na ions in the porous Bi nanostructure? We quantitatively analyzed these issues via experiments and DFT calculations.

3.1. Coalescence of Bi NPs in the presence of solvents

Metal NPs dissolved in liquid media are prone to coalescence to reduce the surface energy when they are separated by a sufficiently small distance [9b]. However, in battery systems, the coalescence tendency of metal NPs may differ depending on the electrolyte solvent because the solvent molecules are polarized and can thus interact with the metal NPs. In general, the surfaces of metal NPs are positively charged[16] and can attract the negatively charged ends of polarized solvent molecules, causing the formation of a solvation layer. This solvation layer plays an important role in determining the coalescence behavior of NPs, such that the thicker the solvation layer, the more difficult it is for the NPs to coalesce. Therefore, comparative studies based on DFT calculations were performed to analyze the effects of various electrolyte solvents on the coalescence of Bi NPs (for the detailed morphologies, dimensions, and charge distributions of the DME, EC, and DEC molecules, see Figure S9, Supporting Information). This was achieved by monitoring the adhesion behaviors of the solvent molecules at the surfaces of the Bi NPs. For this purpose, we placed the DME, EC, and DEC molecules at a position 0.3 nm away from the surface of the Bi NPs and monitored

their movements. The results showed that the molecular DME remained away from the Bi surface, whereas the molecular EC and DEC tended to adhere to the Bi surface (**Figure 4**a and Figure S10, Supporting Information).

Subsequently, we quantitatively analyzed the adsorption tendencies of the solvent molecules to the Bi NPs by evaluating their adsorption energies (Figure 4b). The adsorption energy calculated for molecular DME was small (0.10 eV/atom), whereas the adsorption energies for the EC and DEC molecules were markedly large (0.27 and 0.17 eV/atom, respectively). These results indicate that compared to DME, molecular EC and DEC exhibit greater propensities for the formation of a solvation layer (inset schematic of Figure 4c). Furthermore, because the outer surface of a solvation layer composed of EC and DEC molecules is positively charged, this layer could further attract surrounding ions/molecules. This can cause the formation of a liquid–solid interface similar to the "electrical double layer", which renders adjacent Bi NPs to repel each other, further increasing the interspacing between NPs. Therefore, the solvation layer covering the Bi NPs prevents their coalescence, causing them to be isolated (Figure 4c). Conversely, because of the small adsorption energy of the molecular DME, the DME molecules do not adhere to the surface of the Bi NPs (Figure S10, Supporting Information), which can cause the NPs to evolve into a 3D networked nanostructure after a prolonged time (inset schematic of Figure 4d).

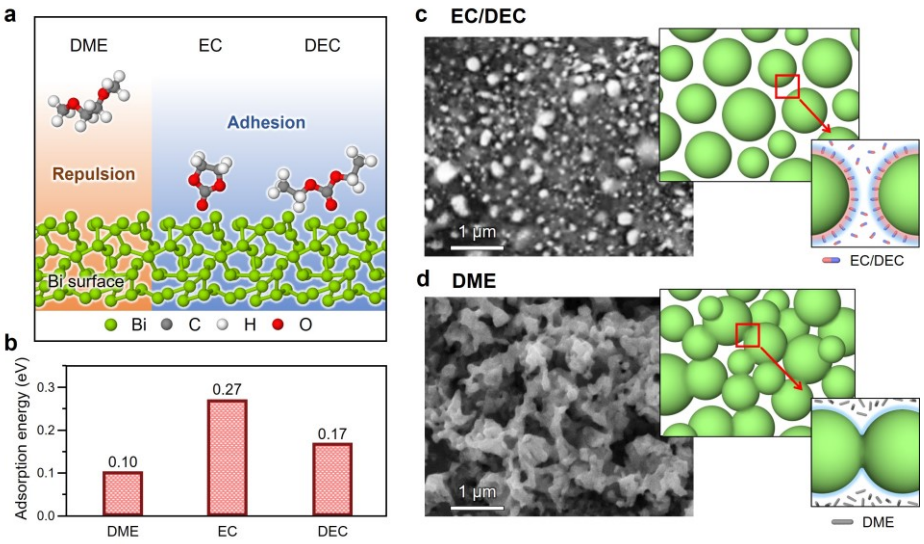

Figure 4. (a) Final stages of DFT calculations performed to replicate interfacial interactions of the Bi surface with EC, DEC, and DME molecules. (b) Adsorption energies calculated for the EC, DEC, and DME molecules upon interaction with the Bi surface. (c) Bi NPs extracted from the 20-times-cycled Na–Bi half-cell with the EC/DEC. The insets show schematics depicting the solvation layer covering the Bi NPs. (d) Porous Bi nanostructure constructed by the coalescence of fragmented Bi NPs in the DME solvent. The inset shows schematics depicting the distribution of the DME molecules around the Bi NPs.

3.2. Electrical conductivity vs. diffusivity relationship

Although the results based on DFT calculations (sec. 3.1.) are instructive for elucidating how fragmented Bi NPs can construct the 3D porous nanostructure in the presence of DME solvent, the results in Figure 3 suggests that the porous nanostructure characterized by a short diffusion distance (x) is not the only factor, which resulted in the

excellent rate capability of the Bi anode. Considering the relationship ($t \propto x^2/D$) supporting the kinetics of diffusion, we consider the Na diffusivity (D) at the Bi anode to be another important factor affecting the rate performance.

Electric charges are stored by the diffusion of carrier ions into the anode, during which various intermediate phases are formed as a result of electrode reactions. Therefore, to understand the origin of the fast kinetics exhibited by the Bi anode, the diffusivities of all the intermediate phases involved in the charging process were measured and compared for the model systems. In this study, only the intermediate phases formed in the Na–Sn, Na–Pb, and Na–Bi systems were considered because the phase transition sequence in the Na–CuS system is still debated[17]. Previous studies based on experiments and calculations showed that the phase transition in the Na–Sn[17a, 18] and Na–Pb[17c] systems proceeds according to Sn → $Na_{0.5}Sn$ → NaSn → $Na_{2.25}Sn$ → $Na_{3.75}Sn$ and Pb → $Na_{0.33}Pb$ → NaPb → $Na_{2.25}Pb$ → $Na_{3.75}Pb$, respectively. *In situ* X-ray diffractometry performed on the Na–Bi system confirmed that the phase transition in this system follows Bi → NaBi → hexagonal Na_3Bi (*h*-Na_3Bi) (Figure S12, Supporting Information), which is consistent with the previous study[19]. Because the diffusivity of the phase is inversely related to the electrical resistivity in the presence of an electric field[7], we first evaluated the Na diffusivities of the phases indirectly by calculating their electrical resistivities (see Methods, Supporting Information). **Figure 5**a shows the electrical resistivities of the intermediate phases formed during the charging (or sodiation) process in the Na–Sn, Na–Pb, and Na–Bi battery systems (for the electronic structures used to calculate the resistivity, see Figure S11, Supporting Information). For the Na–Sn and Na–Pb systems, the phase transitions were characterized by the formation of

phases with high resistivities. This is particularly true for the NaSn and NaPb phases. These phases, which are known as the "Zintl phases", comprise the Sn_4^{4-} and Pb_4^{4-} tetrahedral ionic clusters (insets in Figure 5a) and exhibit high electrical resistivities[20]. Therefore, during charging at high C-rates, these electrically resistive Zintl phases act as the major structure that hinders the transport of Na ions into the anodes and can cause Na depletion at the anodes, which rapidly reduces the charge storage. For the Na–Bi half-cell, two intermediate phases formed: NaBi and Na_3Bi (Figure S12, Supporting Information). Interestingly, unlike NaSn and NaPb, NaBi does not contain Zintl ions (see the inset in Figure 5a) and exhibits high electrical conductivity. The Na_3Bi phase was identified as the hexagonal Na_3Bi[19, 21] (*h*-Na_3Bi, Figure S12, Supporting Information), which is known as a "3D topological Dirac semimetal". *h*-Na_3Bi is also referred to as 3D graphene, because it is a natural 3D counterpart of graphene (inset in Figure 5a)[22] and thus is highly conductive. Therefore, in contrast to the phases formed in the Na–Sn and Na–Pb systems, both NaBi and Na_3Bi can readily transport Na ions into the anode at high C-rates.

Because the phase transition during charging occurs in a sequential manner, the phases with the highest electrical resistivities act as the major structures that control the entire kinetics at the anode. To directly evaluate the Na diffusivities of these phases using DFT calculations, we selected the phases with the highest resistivities (NaSn, NaPb, and NaBi) from their respective systems. We also calculated the Na diffusivities of $Na_{3.75}Sn$, $Na_{3.75}Pb$, and Na_3Bi, because they are the final phases, corresponding to fully sodiated states, covering the outer surface of the active electrode materials. The diffusivities of the phases were evaluated by calculating the vibrational motion of the Na atoms in each phase in terms of the

mean square displacement $\langle r^2 \rangle$. Figure 5b shows the $\langle r^2 \rangle$ vs. time plot evaluated for the Na atoms diffusing into the respective phases. The results showed significantly higher $\langle r^2 \rangle$ values for the NaBi and Na_3Bi phases of the Na–Bi system, confirming the active motion of the Na atoms in these phases. The $\langle r^2 \rangle$ values obtained from the phases were converted into the Na diffusivity (D_{Na}) values according to $D_{Na} = \frac{1}{6}\frac{d}{dt}\langle r^2 \rangle$ (Figure 5c). A comparison showed that the D_{Na} values for the NaBi and Na_3Bi phases were higher than those of other phases in the Na–Sn and Na–Pb systems by more than 5–6 factors of magnitude. The high diffusivities of the NaBi and Na_3Bi phases permits the rapid transport of Na ions to the Bi anode, which explains how the Na–Bi cells could suppress the onset of the DLC.

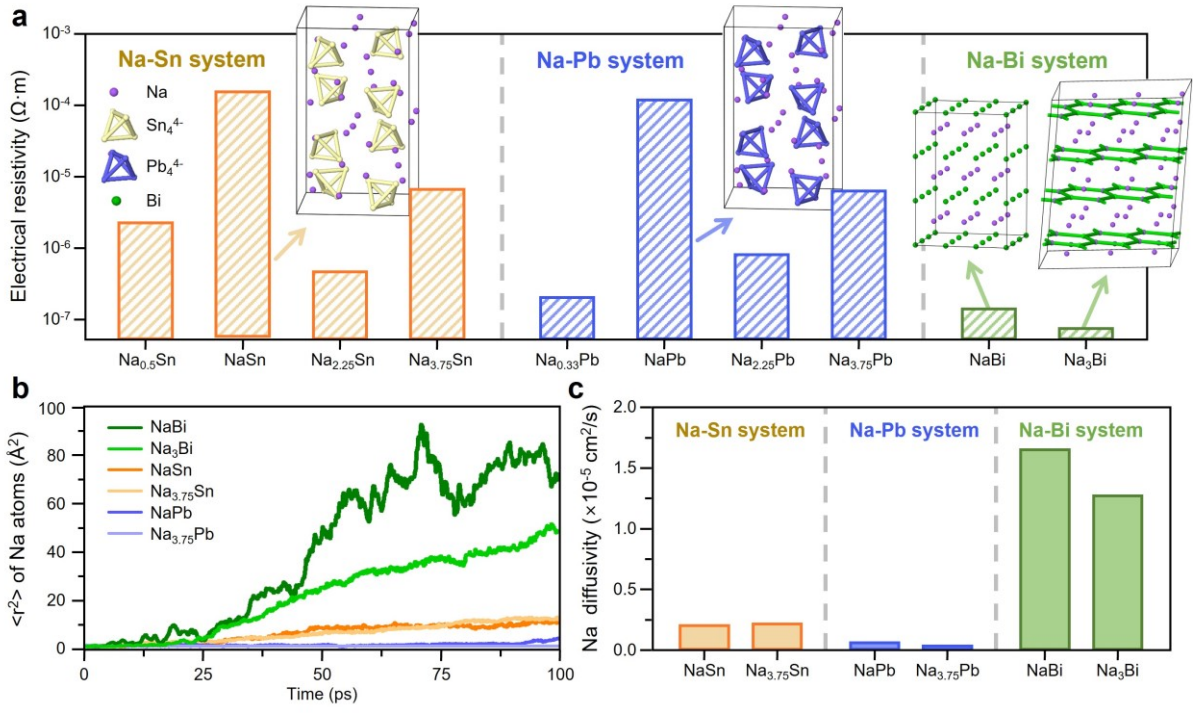

Figure 5. Electrical resistivity vs. diffusivity relation of intermediate phases. (a) DFT calculation results showing electrical resistivities evaluated for various intermediate phases formed in the Na–Sn, Na–Pb, and Na–Bi systems during charging/sodiation, (b) $\langle r^2 \rangle$ values of Na atoms, and (c) Na diffusivities evaluated for NaSn, NaPb, NaBi, $Na_{3.75}Sn$, $Na_{3.75}Pb$, and Na_3Bi phases at 500 K.

3.3.Electrochemical kinetic processes of model systems

Although the resistivity–diffusivity relationship identified using DFT calculations is instructive for elucidating the structural origins responsible for the superior rate performance of the Bi anode, the calculations performed on the model phases were based on the periodic boundary condition. Accordingly, these analyses only determined the bulk properties of the material and did not fully reflect the surface properties of porous nanomaterials, which are characterized by large surface-to-volume ratios.

In a battery system, the mechanisms of the electrochemical reactions (i.e., the charge transfer at the anode) are classified as faradaic and non-faradaic processes[23]. Because the faradaic process stores electric charges through the redox reaction occurring at the interior of the active electrode materials, it is disadvantageous for fast charging in a system that restricts carrier-ion diffusion into the anode[24]. Conversely, the non-faradaic process stores charges on the surface without carrier-ion diffusion[24-25]. Therefore, an anode with a porous nanostructure is advantageous for fast charging when the electrode reactions in this structure follow the non-faradaic process[5a, 10c, 26]. To quantitatively analyze the energy storage

mechanism at the porous nanostructured anodes, cyclic voltammograms were obtained for the Na–Sn, Na–Pb, and Na–Bi systems at different voltage scan rates of 0.6–10 mVs^{-1} (**Figure 6**a–c). The peak current (i) corresponding to the anodic (desodiation) and cathodic (sodiation) reactions is related to the voltage scan rate (v) according to the power law, $i = av^b$, where a and b are constants[27]. The b-value can be obtained from the slope of the log(i) vs. log(v) plot and used to assess the mechanism responsible for the electrochemical reactions. A b-value of 0.5 indicates a faradaic process, whereas a b-value of 1.0 represents a non-faradaic process.

Figure 6d shows the b-values evaluated for the anodic and cathodic peaks measured from the Na–Sn, Na–Pb, and Na–Bi half-cells (for the linear fit of the log(i) vs. log(v) plots, see Figure S13, Supporting Information). Reactions with b-values close to 0.5 limit the entire electrochemical kinetics during sodiation because of the large contribution of the lattice diffusion governed by the faradaic process. Therefore, we compared the smallest b-values evaluated from the sodiation peaks in each battery system: 0.65, 0.57, and 0.81 for the Na–Sn, Na–Pb, and Na–Bi systems, respectively. This indicates that the sodiation process at the Sn and Pb anodes was dominated by the faradaic process, whereas that at the Bi anode was governed by the non-faradaic reaction, causing the Bi anode to display fast kinetics. In summary, the ultrafast sodiation/charging rates of the Bi anodes may arise from the following factors: (1) the short diffusion distance of the Bi nanostructure, (2) the high electrical conductivity of the NaBi and Na_3Bi intermediate phases, and (3) the fast charge storage process occurring at a large surface that is controlled by the non-faradaic reaction.

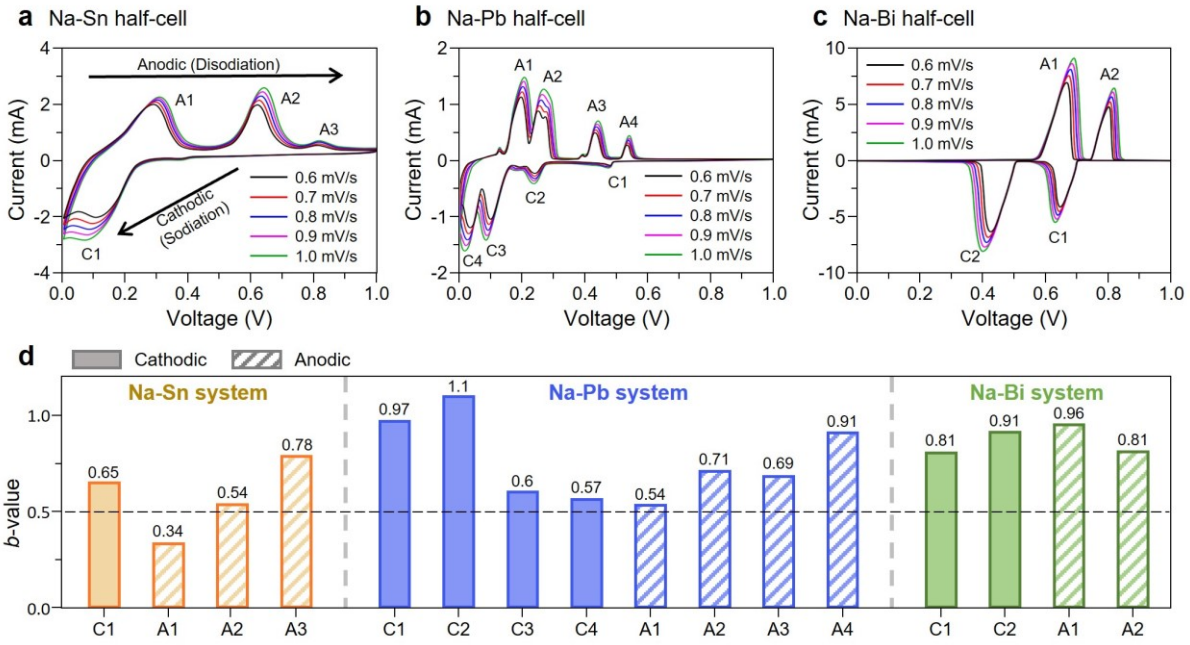

Figure 6. Analysis results of charge storage processes. Cyclic voltammetry curves of (a) Sn, (b) Pb, and (c) Bi anodes measured at different scan rates for Na–Sn, Na–Pb, and Na–Bi half-cells, respectively; and (d) *b*-values evaluated from different current peaks in Na–Sn, Na–Pb, and Na–Bi half-cell systems.

4. Conclusion

In this study, we demonstrated that the seemingly destructive fragmentation behavior of an anode material can be utilized as an effective method to obtain the NPs required for the coalescence process during subsequent battery cycling. The fragmented Bi NPs progressively evolved into a 3D porous nanostructure during cycling in the DME electrolyte. Because a porous Bi nanostructure was obtained by the spontaneous transformation of fragmented NPs

in the DME electrolyte, it is structurally and chemically stable and is characterized by the short diffusion distance. Furthermore, the Bi nanostructure produced the phases with high diffusivity during sodiation, whereas the electrochemical reactions at the surface of the porous Bi nanostructure were dominated by the non-faradaic processes. Such unique features of the porous Bi nanostructure improved the rate performance, practical capacity, and cyclability of the anodes. Combining the experimental and simulation results obtained in this study, it is concluded that the extremely fast-charging rates of the Bi anodes arose from the combined effects of the following factors: (1) the short diffusion distance of the Bi nanostructure, (2) the high diffusivity of the NaBi and Na_3Bi intermediate phases, and (3) the fast charge storage mechanism occurring at a large surface, which was dominated by the non-faradaic reaction. The present findings not only broaden our understanding of the underlying mechanisms of fast-charging anodes, but also provide basic guidelines for finding alloying anodes with simultaneously improved capacity, rate performance, and cyclability.

5. Experimental section

Full experimental procedures are provided in the Supporting Information.

Supporting Information

Supporting Information is available from the Wiley Online Library or from the author.

Acknowledgements

JC is grateful for the financial support from the National Research Foundation of Korea (NRF) grant funded by the Korea government (MEST, NRF-2021R1A2C2009596). YC and DOS are grateful to UK Materials and Molecular Modelling Hub for computational resources, which is partially funded by EPSRC (EP/P020194/1 and EP/T022213/1). Ab initio molecular dynamics calculations were run on ARCHER2 UK National Supercomputing Service (http://www.archer2.ac.uk) via our membership of the UKs HEC Materials Chemistry Consortium (HEC MCC) funded by EPSRC (EP/L000202, EP/R029431).

Author contributions

Young-Hoon Kim and Jae-Hyun An contributed equally to this work.

Conflict of Interest

The authors declare no conflict of interest.

Keywords

sodium-ion batteries, ultrafast charging, bismuth anodes, 3D porous nanostructures, DFT calculations

References

[1] a)S. Komaba, Y. Matsuura, T. Ishikawa, N. Yabuuchi, W. Murata, S. Kuze, *Electrochemistry Communications* **2012**, 21, 65; b)K. Dai, H. Zhao, Z. Wang, X. Song, V. Battaglia, G. Liu, *Journal of Power Sources* **2014**, 263, 276; c)M. Fukunishi, N. Yabuuchi, M. Dahbi, J.-Y. Son, Y. Cui, H. Oji, S. Komaba, *The Journal of Physical Chemistry C* **2016**, 120, 15017; d)C. Kim, K.-Y. Lee, I. Kim, J. Park, G. Cho, K.-W. Kim, J.-H. Ahn, H.-J. Ahn, *Journal of Power Sources* **2016**, 317, 153; e)M. K. Sadan, S.-H. Choi, H. H. Kim, C. Kim, G.-B. Cho, K.-W. Kim, N. Reddy, J.-H. Ahn, H.-J. Ahn, *Ionics* **2018**, 24, 753.

[2] a)R. A. Huggins, *Journal of Power Sources* **1999**, 81, 13; b)A. Magasinski, P. Dixon, B. Hertzberg, A. Kvit, J. Ayala, G. Yushin, *Nature materials* **2010**, 9, 353; c)H. Tavassol, E. M. Jones, N. R. Sottos, A. A. Gewirth, *Nature materials* **2016**, 15, 1182.

[3] a)Y. Liu, N. Zhang, L. Jiao, J. Chen, *Advanced Materials* **2015**, 27, 6702; b)B. Luo, T. Qiu, D. Ye, L. Wang, L. Zhi, *Nano Energy* **2016**, 22, 232; c)Y. Jeon, X. Han, K. Fu, J. Dai, J. H. Kim, L. Hu, T. Song, U. Paik, *Journal of Materials Chemistry A* **2016**, 4, 18306.

[4] a)N. Zhang, C. Sun, Y. Huang, C. Zhu, Z. Wu, L. Lv, X. Zhou, X. Wang, X. Xiao, X. Fan, *Journal of Materials Chemistry A* **2021**, 9, 1812; b)C. Wang, L. Wang, F. Li, F. Cheng, J. Chen, *Advanced Materials* **2017**, 29, 1702212; c)C. Kim, I. Kim, H. Kim, M. K. Sadan, H. Yeo, G. Cho, J. Ahn, J. Ahn, H. Ahn, *Journal of Materials Chemistry A* **2018**, 6, 22809; d)H. Kim, M. K. Sadan, C. Kim, S.-H. Choe, K.-K. Cho, K.-W. Kim, J.-H. Ahn, H.-J. Ahn, *Journal of Materials Chemistry A* **2019**, 7, 16239; e)Z. Li, W. Zhong, D. Cheng, H. Zhang, *Journal of Materials Science* **2021**, 56, 11000.

[5] a)H. Yang, R. Xu, Y. Yao, S. Ye, X. Zhou, Y. Yu, *Advanced Functional Materials* **2019**, 29, 1809195; b)J. Chen, X. Fan, X. Ji, T. Gao, S. Hou, X. Zhou, L. Wang, F. Wang, C. Yang, L. Chen, *Energy & Environmental Science* **2018**, 11, 1218.

[6] C. Heubner, M. Schneider, A. Michaelis, *Advanced Energy Materials* **2020**, 10, 1902523.

[7] P. J. Tumidajski, A. Schumacher, *Cement & concrete research* **1996**, 26, 1301.

[8] J. Sottmann, M. Herrmann, P. Vajeeston, Y. Hu, A. Ruud, C. Drathen, H. Emerich, H. Fjellvag, D. S. Wragg, *Chemistry of Materials* **2016**, 28, 2750.

[9] a)H. Shirai, M. T. Nguyen, Y. Ishida, T. Yonezawa, *Journal of materials chemistry C* **2016**, 4, 2228; b)C. Cao, K. Huang, J. Shi, D. Zheng, W. Wang, L. Gu, H. Bai, *Nature communications* **2019**, 10, 1; c)J. M. Yuk, M. Jeong, S. Y. Kim, H. K. Seo, J. Kim, J. Y. Lee, *Chemical Communications* **2013**, 49, 11479; d)J. M. Yuk, J. Park, P. Ercius, K. Kim, D. J. Hellebusch, M. F. Crommie, J. Y. Lee, A. Zettl, A. P. Alivisatos, *Science* **2012**, 336, 61.

[10] a)L. Wang, C. Wang, F. Li, F. Cheng, J. Chen, *Chemical Communications* **2018**, 54, 38; b)H. Yang, L.-W. Chen, F. He, J. Zhang, Y. Feng, L. Zhao, B. Wang, L. He, Q. Zhang, Y. Yu, *Nano letters* **2019**, 20, 758; c)P. Xiong, P. Bai, A. Li, B. Li, M. Cheng, Y. Chen, S. Huang, Q. Jiang, X. H. Bu, Y. Xu, *Advanced Materials* **2019**, 31, 1904771; d)Q. Zhang, J. Mao, W. K. Pang, T. Zheng, V. Sencadas, Y. Chen, Y. Liu, Z. Guo, *Advanced Energy Materials* **2018**, 8, 1703288; e)D. Su, S. Dou, G. Wang, *Nano Energy* **2015**, 12, 88; f)S. Liu, Z. Luo, J. Guo, A. Pan, Z. Cai, S. Liang, *Electrochemistry Communications* **2017**, 81, 10; g)J. Xiang, Z. Liu, T. Song, *ChemistrySelect* **2018**, 3, 8973; h)F. Yang, F. Yu, Z. Zhang, K. Zhang, Y. Lai, J. Li, *Chemistry–A European Journal* **2016**, 22, 2333.

[11] a)J.-H. Park, Y.-S. Choi, Y.-W. Byeon, J.-P. Ahn, J.-C. Lee, *Nano Energy* **2019**, 65, 104041; b)Y.-S. Choi, Y.-W. Byeon, J.-H. Park, J.-H. Seo, J.-P. Ahn, J.-C. Lee, *ACS applied materials & interfaces* **2018**, 10, 560.

[12] a)S. Swaroop, M. Kilo, C. Argirusis, G. Borchardt, A. H. Chokshi, *Acta materialia* **2005**, 53, 4975; b)H.-J. Lee, S.-H. Kim, J.-C. Lee, *Scripta Materialia* **2016**, 115, 33.

[13] Y. W. Byeon, J. P. Ahn, J. C. Lee, *Small* **2020**, 16, 2004868.

[14] J.-H. Park, Y.-S. Choi, C. Kim, Y.-W. Byeon, Y. Kim, B.-J. Lee, J.-P. Ahn, H. Ahn, J.-C. Lee, *Nano Letters* **2021**, 21, 9044.

[15] Y. S. Choi, D. O. Scanlon, J. C. Lee, *Advanced Energy Materials* **2021**, 11, 2003078.

[16] Z. Abbas, C. Labbez, S. Nordholm, E. Ahlberg, *The Journal of Physical Chemistry C* **2008**, 112, 5715.

[17] a)Y.-S. Choi, Y.-W. Byeon, J.-P. Ahn, J.-C. Lee, *Journal of Materials Chemistry A* **2018**, 6, 9428; b)A. Darwiche, R. Dugas, B. Fraisse, L. Monconduit, *Journal of Power Sources* **2016**, 304, 1; c)L. Ellis, B. Wilkes, T. Hatchard, M. Obrovac, *Journal of The Electrochemical Society* **2014**, 161, A416.

[18] B. Zhang, G. Rousse, D. Foix, R. Dugas, D. A. D. Corte, J. m. Tarascon, *Advanced Materials* **2016**, 28, 9824.

[19] C.-H. Lim, B. Selvaraj, Y.-F. Song, C.-C. Wang, J.-T. Jin, S.-S. Huang, C.-H. Chuang, H.-S. Sheu, Y.-F. Liao, N.-L. Wu, *Journal of Materials Chemistry A* **2017**, 5, 21536.

[20] G. Seifert, R. Kaschner, M. Schöne, G. Pastore, *Journal of Physics: Condensed Matter* **1998**, 10, 1175.

[21] H. Gao, W. Ma, W. Yang, J. Wang, J. Niu, F. Luo, Z. Peng, Z. Zhang, *Journal of Power Sources* **2018**, 379, 1.

[22] Z. Liu, B. Zhou, Y. Zhang, Z. Wang, H. Weng, D. Prabhakaran, S.-K. Mo, Z. Shen, Z. Fang, X. Dai, *Science* **2014**, 343, 864.
[23] a)A. V. Da Rosa, J. C. Ordonez, *Fundamentals of renewable energy processes*, Academic Press, **2021**; b)P. Biesheuvel, S. Porada, J. Dykstra, *arXiv preprint arXiv:1809.02930* **2018**.
[24] H. Huang, M. Niederberger, *Nanoscale* **2019**, 11, 19225.
[25] Y. Jiang, J. Liu, *Energy & Environmental Materials* **2019**, 2, 30.
[26] H. Yue, Z. Shi, L. Wang, X. Li, H. Dong, Y. Yin, S. Yang, *Journal of Alloys & Compounds* **2017**, 723, 1018.
[27] H. Lindström, S. Södergren, A. Solbrand, H. Rensmo, J. Hjelm, A. Hagfeldt, S.-E. Lindquist, *The Journal of Physical Chemistry B* **1997**, 101, 7717.

Journal's Table of Contents (ToC)

Toc text

With the difficulty in simultaneously achieving a large capacity, ultrafast charging capability, and long cycling stability in a battery anode, we present a bulk Bi anode for Na-ion batteries that provide a simple yet practical route to address this issue without using expensive nanoscale materials and additional complex modifications.

Toc figure